IEEE Access
Multidisciplinary | Rapid Review | Open Access Journal

Received January 7, 2020, accepted January 30, 2020, date of publication February 12, 2020, date of current version March 2, 2020.

Digital Object Identifier 10.1109/ACCESS.2020.2973173

Compliant Control of Single Tendon-Sheath Actuators Applied to a Robotic Manipulator

MENG YIN[1,2,3], HAOTING WU[1,2,4], ZHIGANG XU[1,2], WEI HAN[1,2,4], AND ZHILIANG ZHAO[1,2,4]

[1]Shenyang Institute of Automation, Chinese Academy of Sciences, Shenyang 110016, China
[2]Institutes for Robotics and Intelligent Manufacturing, Chinese Academy of Sciences, Shenyang 110169, China
[3]University of Chinese Academy of Sciences, Beijing 100049, China
[4]School of Mechanical Engineering and Automation, Northeastern University, Shenyang 110169, China

Corresponding author: Meng Yin (yinmenglz@163.com)

ABSTRACT Tendon-sheath actuators (TSAs), similar to Bowden cable-based series elastic actuators (SEAs), have a wide range of applications in robots. However, when applying them to manipulators, force sensors cannot be mounted due to limited space. Therefore, this paper proposes a new method for compliant control based on a dual encoder, and the existing transmission model was improved by considering the joint torque. To validate the proposed method, experimental setups composed of a motor, a tendon-sheath component, a robotic joint, force sensors, and position sensors are established. The transmission processes are interpreted clearly through a position control mode. Parameter identifications without external disturbance force are conducted to acquire the ideal transmission model, and the error value between the experiment data and the fitted curve is measured. The availability of the presented scheme is verified by compliant control experiments, including collision detection and hand guiding, and the frequency characteristics of the actuator are analyzed. The results show that the function can be realized without force and torque sensors during the whole process.

INDEX TERMS Tendon-sheath actuators, robotic manipulator, compliant control, position transmission model, parameter identifications, series elastic actuators, transmission characteristic.

I. INTRODUCTION

A tendon-sheath actuator (TSA), as a kind of series elastic actuator (SEA) [1], can transfer displacement between an internal steel wire and its outer sheath. It provides a valid yet straightforward solution for remote transmission through a tortuous narrow space. As a flexible transmission pathway, it can simplify a mechanical structure and make a system lighter. These actuators can be installed away from a manipulator at a convenient location, which shows promising potential for practical applications. However, the sensors are not always easily affixed due to limited geometric size. Based on the volume of a robotic joint, the existing applications of tendon-sheath actuators can be divided into two categories.

One category is applications on dexterous hands and surgical robots, which is characterized by limited space at the joint side. The flexible cable moves a small distance, and there is enough space at the driver side. Therefore, the tension sensor and encoder are typically installed at the driver side. Previous research on these applications mainly concentrates on the transmission characteristics, force estimations, and compensation controls of TSAs. Kaneko et al. [2], [3] applied TSAs to actuate a robotic finger joint. They described the transmission characteristic using a Coulomb-based friction model. Experiments verified the backlash behavior and nonlinearities of the system. TSAs were used on surgical robots by Phee *et al.* [4], [5]. A method to estimate the force on the joint side and the elongation of the tendon was presented using only a force and position sensor on the motor side. The error was measured under the assumption that the shape of the sheath remains the same.

The other category is applications on rehabilitation robots and exoskeleton [6], which are characterized by sufficient space for the encoder to be installed at the joint side and the driver side. However, the flexible cable moves at a greater distance, so the tension sensor needs a larger space and is not easily installed. Torque control and compliant control based on TSAs have been studied in recent works. Kong *et al.* [7], [8] applied TSAs to a rehabilitation system. A sensor-fusion method based on a kinematic Kalman filter

The associate editor coordinating the review of this manuscript and approving it for publication was Giambattista Gruosso.

with accelerometers was proposed to determine the reference trajectory of the motor in real time. A cable-driven actuating system realized a precise force-mode actuation. Agarwal *et al.* [9], [10] realized torque control by measuring the deflection of the spring. The deflection was estimated by the displacement of the actuator and the joint. It was assumed that the stretch in the cable was negligible. Experiments were carried out to quantify the torque tracking performance of the SEA. Wu *et al.* [11], [12] designed an upper limb exoskeleton robot with a function of gravity balance. A fuzzy sliding mode admittance control strategy was applied to meet the training needs of different patients, and the patient participation and human-computer interaction performance were improved. Vallery et al [13], [14] developed a model to describe the basic dynamics of a Bowden cable-based actuation system for design purposes. By combining compliant actuation and impedance control, interaction forces between the exoskeleton and humans were controlled towards zero in the patient-in-charge mode.

With the development of humanoid and service robots, the humanoid lightweight manipulator has become an important component in the robot field. The human arm can sustain a large load and has a compact structure, which presents new challenges for the design of humanoid manipulators. One option is to use a traditional motor and reducer, such as ASIMO [15] and Sophia [16], which offers an appearance similar to the human arm but sustains a small load. Another option is to use a permanent magnet synchronous motor and harmonic reducer, such as ABB-YuMi [17], DLR-Justin [18], Rethink-Saywer [19] and Kinova-Jaco [20]. They can sustain a large load but have a higher price and a less anthropomorphic appearance. Flexible cable drives have been used in mechanical arms, such as WAM [21] and LIMS2 [22]. The existing flexible cable mechanisms mainly realize long-distance transmission through a transmission wheel, which is complex in structure, resulting in high manufacturing and system maintenance costs. To make the manipulator lighter and more anthropomorphic, as shown in Fig. 1, we have designed a 7-DOF manipulator based on TSAs. A video link of physical experiments can be provided.[1]

[1]https://youtu.be/ggHBsV4BCO0

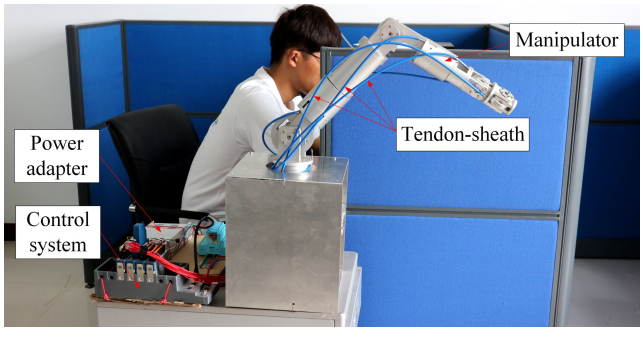

FIGURE 1. 7-DOF manipulator based on TSAs.

With the increasing complexity of tasks faced by robots, only using position control cannot meet the needs of practical applications, such as polishing, parts assembly, and work requiring human-robot cooperation [23], [24]. Compliant control that obtains better contact performance has become a significant research direction in the field of robotics [25]–[28]. The concept of compliant control was introduced by Calanca *et al.* [29]. They proposed a complete and coherent overview of existing compliant control solutions for series elastic joints, and they highlighted the advantages of impedance control based on positive acceleration feedback. According to the ISO 10218-1/2 standard [30], [31], collision detection and hand guiding are representative applications in robot collaborations with humans. Haddadin *et al.* [32], [33] presented new torque-controlled robots. To enable robots to act in unstructured environments and physically interact with humans, collision detection was used, and some application examples were highlighted. Min *et al.* [34] presented a collision detection method based on the vibrations caused by collisions. A BP neural network was used to analyze the vibration signals, and the experiments showed that detection could be realized by the frequency-domain and time-domain features of collision. Fujii *et al.* [35], [36] applied a hand-guided robot system to transportation and assembly work at automobile factories. Heavy or large parts could be moved to target locations where humans could operate the industrial manipulator directly and work collaboratively. A sensorless control scheme for hand guiding was proposed by Zhang *et al.* [37]. The external force estimation error could be calculated by the virtual mass and friction mode, and the proposed control scheme was verified on a 6-DOF industrial robot.

Considering the above studies, a new approach for the compliant control of single TSAs is presented based on the position transmission model in this paper. An experimental device is designed to test the presented transmission model. The transmission process is analyzed during position control mode by a sinusoidal signal. Parameter identification is used to determine the position transmission model based on dual encoders installed on the drive motor and the actuated joint. The performance of the presented method is evaluated by compliant control experiments. The compliant control method can be applied in a manipulator actuated by a tendon sheath, which is instructive for applications using a rehabilitation robot and an exoskeleton.

II. TRANSMISSION MODEL

A. SINGLE TENDON-SHEATH TRANSMISSION

The relationship between the input force and the output force can be established on the basis of the LuGre friction model. However, the model needs long calculation time and a complex derivation process [38]. Therefore, a transmission model based on static Coulomb friction is adopted here.

A small segment of a single tendon-sheath transmission system is illustrated in Fig. 2. The length of the element is dx,

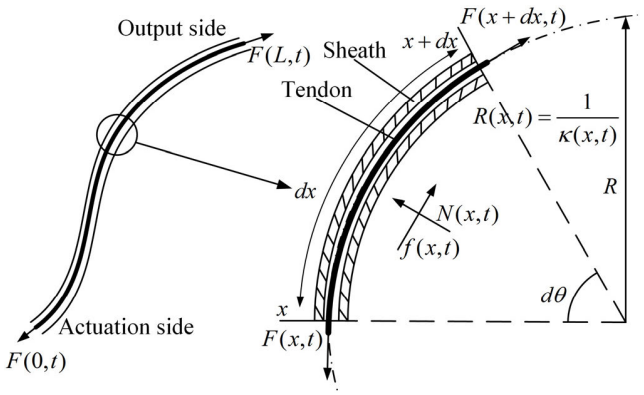

FIGURE 2. An infinitesimal element of single TSAs.

and we define the position of a tendon-sheath microsegment using arc length x. When dx is small enough, the quasi-static equilibrium of a segment $[x, x+dx]$ in the tangential direction is calculated as

$$dF(x,t) = \text{sgn}(\dot{x}) f(x,t) \tag{1}$$

In the normal direction, we can obtain

$$N(x,t) = F(x,t)d\theta \tag{2}$$

According to the Coulomb friction model, the friction of the rope microelement is

$$f(x,t) = \mu F(x,t)\frac{dx}{R} \tag{3}$$

where $N(x,t)$, $F(x,t)$, $f(x,t)$, R, and $\mathrm{d}\theta$ are the normal force, the tension of the tendon, the friction force, the radius, and the center angle corresponding to dx, respectively; μ is the coefficient of friction; and t is the time.

From (1), we can obtain

$$\frac{dF(x,t)}{dx} = \frac{\text{sgn}(\dot{x}) f(x,t)}{dx} \tag{4}$$

Combining (3) and (4), we obtain

$$\frac{F'(x,t)}{F(x,t)} = \frac{\text{sgn}(\dot{x})\mu}{R} \tag{5}$$

where $\text{sgn}(\dot{x})$ is the sign function related to the movement velocity $\dot{x}$ and $F'(x,t)$ represents a partial differential with regard to x. If the microsegment of the tendon has a movement from the joint side to the actuation side, we have $\dot{x} > 0$ and $\text{sgn}(\dot{x}) = 1$. If the direction of movement is reversed, we have $\dot{x} < 0$ and $\text{sgn}(\dot{x}) = -1$.

By integrating over the segment $[x, x+dx]$, we obtain

$$F(x+dx,t) = F(x,dt)\exp\left[\text{sgn}(\dot{x})\mu\kappa(x,t)dx\right] \tag{6}$$

where $\kappa(x,t)$ is the curvature at position x. Then, the force at the output side is bound up with the force at the actuation side by

$$F(L,t) = F(0,t)\cdot\Phi \tag{7}$$

where

$$\Phi \triangleq \begin{cases} \Phi_p = \exp\left[\mu\int_0^L \kappa(x,t)dx\right], & \dot{x} > 0 \\ \Phi_r = \exp\left[-\mu\int_0^L \kappa(x,t)dx\right], & \dot{x} < 0 \end{cases} \tag{8}$$

The tendon is stretched when it is tightened. Under the assumption that the extension is within the elastic limit, the elongation of the tendon can be expressed by Hook's law:

$$\begin{aligned}\Delta L(t) &= \int_0^L \frac{F(x,t)}{EA}dx \\ &= \frac{F(0,t)}{AE}\int_0^L \exp\left[\text{sgn}(\dot{x})\mu\int_0^L \kappa(x,t)dx\right]dx\end{aligned} \tag{9}$$

When there is a static relationship between the tendon and the sheath, the elongation at position L is constant, i.e., $\Delta L(L,t) = \Delta L(L,t^-)$. Thus, the elongation of the tendon can be expressed as

$$\Delta L(t) = \begin{cases} \Theta\cdot F(L,t), & \dot{x} \neq 0 \\ \Delta L(t^{-1}), & \dot{x} = 0 \end{cases} \tag{10}$$

where

$$\Theta \triangleq \begin{cases} \Theta_p = \frac{1}{AE\Phi}\int_0^L \exp\left[\mu\int_0^L \kappa(x,t)dx\right]dx, & \dot{x} > 0 \\ \Theta_r = \frac{1}{AE\Phi}\int_0^L \exp\left[-\mu\int_0^L \kappa(x,t)dx\right]dx, & \dot{x} < 0 \end{cases} \tag{11}$$

B. POSITION TRANSMISSION MODEL

A single TSA can only provide one-direction actuation in practical applications, and the joint is typically pulled back by the recovery of a spring in existing studies [39]. However, the elastic component will be unnecessary for the pitch joint. When the tendon pulls the joint, the gravitational potential energy will be stored. When the tendon is released, the joint will be pulled back under the action of gravity.

As shown in Fig. 3, a robotic pitch joint can be remotely actuated by single TSAs. The tendon is fixed to the pulleys on the actuated joint and the drive motor in a pull–pull

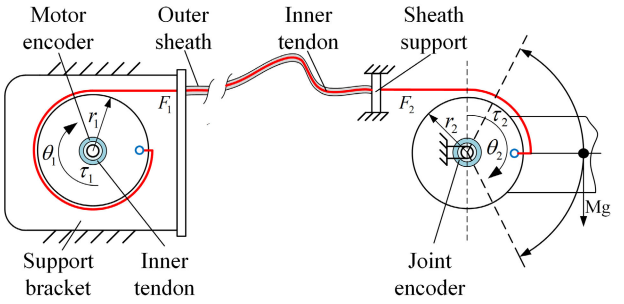

FIGURE 3. Schematic of single TSA.

configuration. The mechanical displacement is transmitted by a pulling force between the outer sheath and the inner tendon. Two encoders are respectively mounted on the motor and the joint, and the joint encoder is a small-sized magnetic encoder adapted to the limited space. r_1 and r_2 are the radii of pulleys on the motor and the joint. θ_1, θ_2, ω_1, and ω_2 are the rotational angles and speeds of the drive motor and the actuated joint. F_1 and F_2 denote the forces of the tendon on the motor side and the joint side. τ_1 is the input torque applied by the drive motor, and τ_2 is the output torque acting on the robotic joint. If the motor and the joint rotate clockwise in a positive direction, we define $\omega > 0$ and $\text{sgn}(\omega) = 1$. If the motor and the joint rotate counter-clockwise in a negative direction, we define $\omega < 0$ and $\text{sgn}(\omega) = -1$. Here, ω includes ω_1 and ω_2. The drawback of the system is that the actuated joint only moves during the range near π on the right of the dotted line shown in Fig. 2, but this is sufficiently useful for the robotic pitch joints. Single TSAs can simplify the structure of the manipulator better than double TSAs, and the initial position can be adjusted by the motion of the motor to replace the pre-tension device.

According to the expressions of elongation in (9), ΔL is constant when there is a relatively static relationship between the tendon and the sheath. Therefore, while the tendon is in the state of movement, we can rewrite (10) as

$$\Delta L(t) = \Theta \cdot F_2(t) \tag{12}$$

It is assumed that the tendon elongation is always within elastic limitation, and the starting values of the motor angle θ_1 and the joint angle θ_2 are equivalent in this system. The elongation of tendons can be calculated by

$$\Delta L(t) = r_2\theta_2(t) - r_1\theta_1(t) \tag{13}$$

There are no components to measure the torque and the force in the system, but when the load or the torque acting on the joint varies, the relationship between θ_1 and θ_2 will also change. To monitor the joint torque, by combining (12) and (13), the motor angle can be expressed by

$$\theta_1(t) = \frac{r_2}{r_1}\theta_2(t) - \frac{\Theta}{r_1}F_1(t) \tag{14}$$

The motor encoder is calibrated before installation, and the error in measurement can be ignored. The joint magnetic encoder is installed on-site, and there is no systematic calibration. Relevant compensation methods were studied [40], [41], and we used a second-order function to compensate for the error directly:

$$\theta_2 = a_2\hat{\theta}_2^2 + b_2\hat{\theta}_2 + c_2 \tag{15}$$

where $\hat{\theta}_2$ is the feedback value of the joint magnetic encoder, and a_2, b_2, and c_2 are compensation coefficients.

The joint is connected to the load, and the rotational speed of the joint is limited. The effects of acceleration are negligible; thus, we can obtain

$$\tau_2 = Mgl\cos\{\theta_2(t)\} \tag{16}$$

Therefore,

$$F_1(t) = \frac{Mgl}{r_2}\cos\{\theta_2(t)\} \tag{17}$$

According to the Taylor expansion of trigonometric functions, (17) can be transformed by

$$F_1(t) = \frac{Mgl}{r_2}(1 - \frac{\theta_2^2(t)}{2!} + \cdots) \tag{18}$$

Combining (14), (15) and (17), θ_1 can be estimated by

$$\theta_1(t) \cong P\hat{\theta}_2^2 + Q\hat{\theta}_2 + M \tag{19}$$

where

$$P \triangleq \begin{cases} P_p = \dfrac{r_2a_2}{r_1} + \dfrac{\Theta_pMgl}{2r_1r_2}\left(b_2^2 + 2a_2c_2\right), & \omega_2 > 0 \\ P_r = \dfrac{r_2a_2}{r_1} + \dfrac{\Theta_rMgl}{2r_1r_2}\left(b_2^2 + 2a_2c_2\right), & \omega_2 < 0 \end{cases} \tag{20}$$

$$Q \triangleq \begin{cases} Q_p = \dfrac{r_2b_2}{r_1} + \dfrac{2b_2c_2\Theta_pMgl}{2rr_2}, & \omega_2 > 0 \\ Q_r = \dfrac{r_2b_2}{r_1} + \dfrac{2b_2c_2\Theta_rMgl}{2rr_2}, & \omega_2 < 0 \end{cases} \tag{21}$$

$$M \triangleq \begin{cases} M_p = \dfrac{r_2c_2}{r_1} + \dfrac{\Theta_pMgl}{r_1r_2}\left(c_2^2 - 1\right), \omega_2 > 0 \\ M_r = \dfrac{r_2c_2}{r_1} + \dfrac{\Theta_rMgl}{r_1r_2}\left(c_2^2 - 1\right), \omega_2 < 0 \end{cases} \tag{22}$$

From (20), (21) and (22), we can see that the transmission characteristics are affected by factors such as tendon radius, motion velocity and total bending angle. When the system runs normally with a fixed sheath shape, the torque acting on the joint will be the only factor affecting transmission characteristics, so torque can be detected in real time by the position transmission model.

III. MODEL VALIDATION

Experiments are conducted to validate the position transmission model. The experimental device is depicted in Fig. 4, and Fig. 5 shows the experimental schematic diagram. The system includes a robotic joint made of duralumin material, a motor (with a drive torque of 38 N · m) as the actuator,

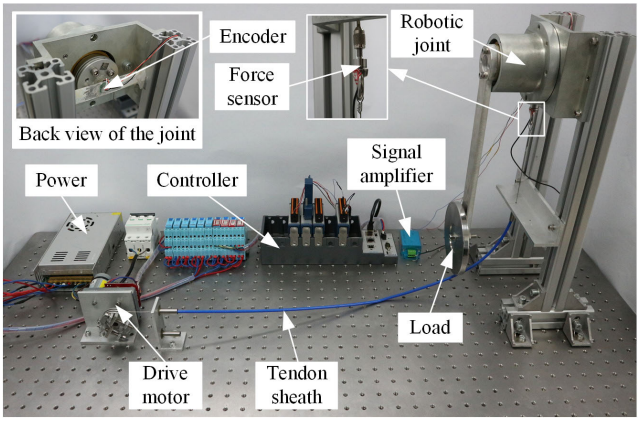

FIGURE 4. Experimental setup for transmission model validation.

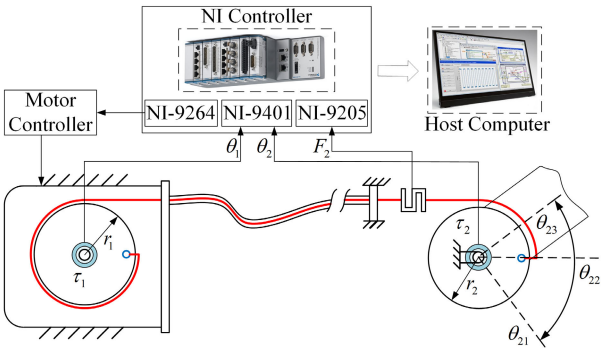

FIGURE 5. Schematic of torque estimation model validation setup.

a single tendon sheath and a force sensor. The tendons used in the transmission system are wires made of stainless steel with a radius of 0.6 mm. The outer sheaths have an inner radius of 1 mm and are tightly wound springs made from rectangular steel wire. The sheath and tendon are 0.8 and 1.2 m in length. The joint is connected to a load of 1 kg.

The distal and proximal ends of the tendon are fixed to the pulleys on the joint side and the actuation side. The robotic joint is mounted on precision bearings to reduce the effect of rotating friction. The whole bending angle of the tendon sheath is designed to $\pi/2$ rad. The radii of the driver and driven pulleys are 20 mm and 25 mm. The control system uses an NI-cRIO-9067 as the slave computer. The rotary displacement of the motor and the joint are measured by encoders and inputted into the NI-9401 module. The force of the tendon on the joint side is measured by a load cell (DYMH-10Kg) and inputted into the NI-9205 module by the signal amplifier. The motion control signal is outputted to the drive motor by the NI-9264 module. The control program is first written by LabVIEW software on the host computer and then downloaded to the slave computer running the real-time system through the Can interface for execution. The frequency of real-time feedback and data monitoring is set to 1 kHz.

During the validation experiments, the drive motor moves to follow the position command of the sinusoidal signal $\theta_1 = \pi/4\sin(\pi/45t\text{-}\pi/2)$rad. Fig. 6 shows the comparison between the position of the servo motor and the joint during a period of 100 s, which clarifies the whole motion process. The characteristics of position transmission are displayed in Fig. 6. To understand the model better, the transmission process can be divided into several phases:

A. The motor rotates counterclockwise and overcomes the frictional resistance, and the joint angle θ_2 increases from θ_{21} to θ_{22} in the negative direction.
B. The actuator overcomes the frictional resistance, and the joint angle θ_2 keeps increasing from θ_{22} to θ_{23} in the negative direction.
C. The drive motor begins to rotate clockwise, and the actuator cannot overcome the friction. Therefore, the system remains static, and the joint angle θ_2 remain constant.

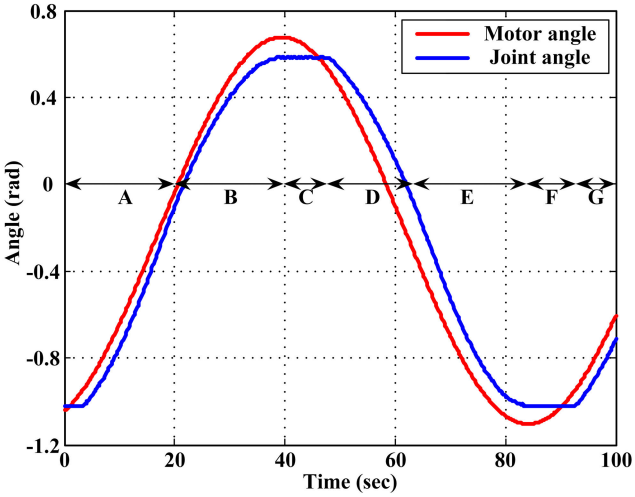

FIGURE 6. Experimental results of position transmission.

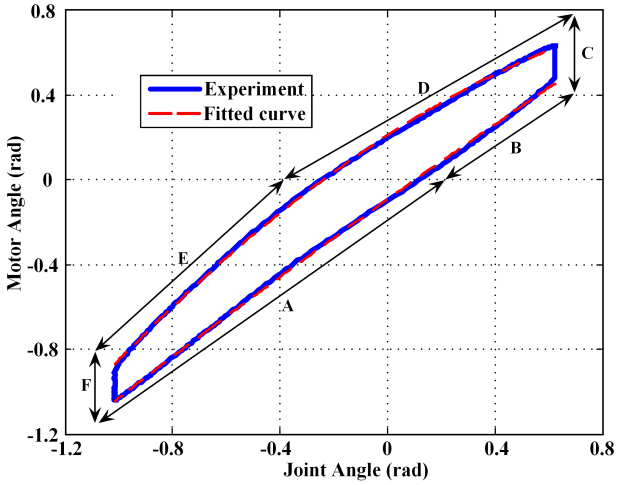

FIGURE 7. Relationship between the motor angle and the joint angle.

D. The drive motor overcomes the frictional force between the tendon and the sheath, making the joint rotate clockwise, and the backlash offset is entirely compensated. The joint angle θ_2 decreases from θ_{23} to θ_{22} in the positive direction.
E. The drive motor keeps rotating clockwise, and the joint angle θ_2 keeps decreasing from θ_{22} to θ_{23} in the positive direction.
F. The drive motor begins to rotate counterclockwise, and the backlash offset cannot be completely compensated. The actuator cannot overcome the friction, so the system remains stationary. The joint angle θ_2 remains constant.
G. Repeat phase A.

The rotation of the joint in the negative direction includes phase A and phase B. The rotation of the joint in the positive direction includes phase D and phase E. The joint torque and the joint angle maintain their previous values in phase C and phase F. Therefore, the position transmission model in the state of motion can be rewritten as two different functions.

As shown in Fig. 7, the fitted value of the motor angle can be obtained using (19), and the motor angle θ_1 can be

calculated by

$$\theta_1(t) = \begin{cases} -0.244\hat{\theta}_2^2 + 0.818\hat{\theta}_2 + 0.212, & \omega_2 > 0 \\ -0.036\hat{\theta}_2^2 + 0.900\hat{\theta}_2 - 0.091, & \omega_2 < 0 \end{cases} \quad (23)$$

It is obvious that the motor angles acquired by the experiment and the fitted curve are consistent, and force and torque sensors are not required for the calibration process to obtain (23). A change in torque will affect the transmission characteristics. The method used to estimate the torque by the elongation of the tendon in the system is feasible, which provides a new approach to monitor the torque by the change rule of the motor angle. The following content will further verify the effectiveness of this method.

IV. MODEL PARAMETER IDENTIFICATIONS

To measure the maximal error between the experimental value and the estimated value, model parameter identifications are presented to obtain the constants Q, P, and M in (19). Fig. 8 shows the experimental setup, and a schematic diagram of parameter identification is displayed in Fig. 9. The load cell is taken away, and the sheath is surrounded by a circular plate with constant radius r_p. The position command of sinusoidal wave motion is inputted into the drive motor. The experiments are conducted under different working conditions.

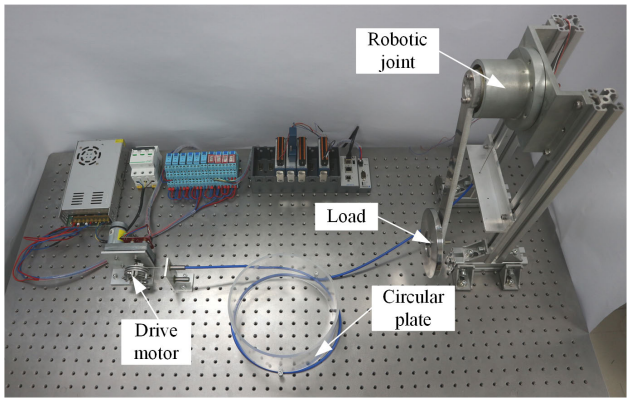

FIGURE 8. Experimental setup for model parameter identification.

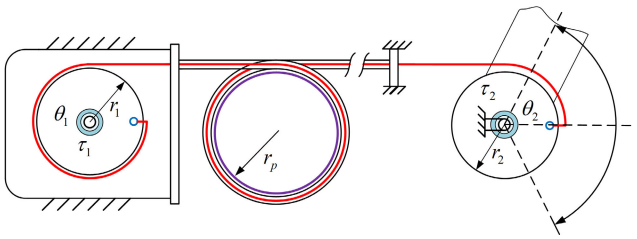

FIGURE 9. Schematic of parameter identification.

The characteristics of position transmission under different bending radii are shown in Fig. 10(a). Different circular plates with radii of 40, 50, and 60 mm were applied while the tendon sheath was always wound to a constant whole bending angle of π. We can see that the variation of bending radii has little influence on position transmission, and the maximal error between estimated values and experimental values is 0.021 rad. The characteristics of position transmission under different tendon radii R_d are depicted in Fig. 10(b). In this experiment, different tendons with radii of 1, 1.2, and 1.5 mm were applied while the tendon sheath was always wound to a constant whole bending angle of π. The results obtained show that the variation of tendon radii has little effect on position transmission, and the maximal error is 0.027 rad.

The characteristics of position transmission under different motion velocities are illustrated in Fig. 11(a). The tendon sheath has a whole bending angle of π and a radius of 50 mm, and the motor moves at different speeds of 0.02, 0.04, and 0.06rad/s. When the speed increases, the characteristics of the position transmission have an apparent change; the identified parameter for different motion velocity is shown in Table 1. The table reveals that the maximal error between the estimated and experimental values is 0.045rad, and the increase in motion velocity can make the error become smaller.

TABLE 1. Identified parameters for different motion velocity.

Motion Velocity	Parameters	P	Q	M	M.E. (rad)
0.02	R.C.	-0.145	0.920	0.225	0.024
	R.A.	-0.099	0.914	0.019	0.021
0.04	R.C.	-0.208	0.912	0.308	0.034
	R.A.	-0.033	0.911	-0.055	0.044
0.06	R.C.	-0.251	0.897	0.361	0.054
	R.A.	-0.012	0.904	-0.116	0.055

R.C.= Rotate Clockwise; R.A.= Rotate Counterclockwise; M.E.= Maximal Error.

Fig. 11(b) shows the characteristics of position transmission under different bending angles. The whole bending angles of the tendon sheaths are designed to $\pi/2$, π, and $3\pi/2$ with a constant bending radius of 50 mm; the identified parameters for different motion velocity are shown in Table 2. It can be concluded that the maximal error is 0.034rad, and there is a negative correlation between the error and bending angles. The tendon sheath used in the experiments is a kind

TABLE 2. Identified parameters for different bending angles.

Bending Angle	Parameters	P	Q	M	M.E. (rad)
$\pi/2$	R.C.	-0.208	0.916	0.301	0.033
	R.A.	-0.030	0.913	-0.063	0.034
π	R.C.	-0.266	0.911	0.361	0.031
	R.A.	-0.055	0.893	-0.123	0.028
$3\pi/2$	R.C.	-0.307	0.920	0.414	0.026
	R.A.	-0.048	0.883	-0.171	0.024

R.C.= Rotate Clockwise; R.A.= Rotate Counterclockwise; M.E.= Maximal Error.

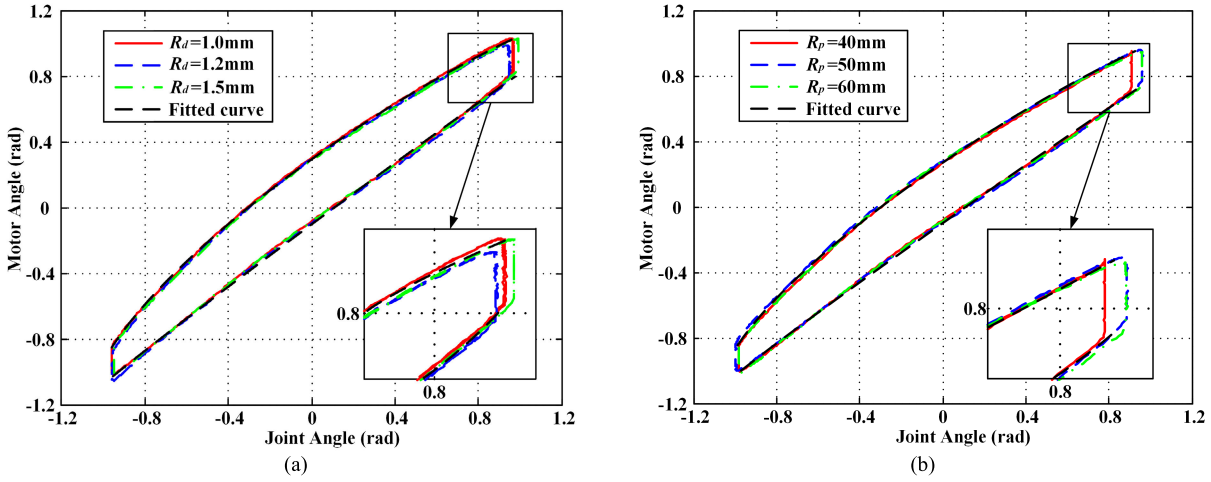

FIGURE 10. Parameter identification under different conditions. (a) Plate radii. (b) Tendon radii.

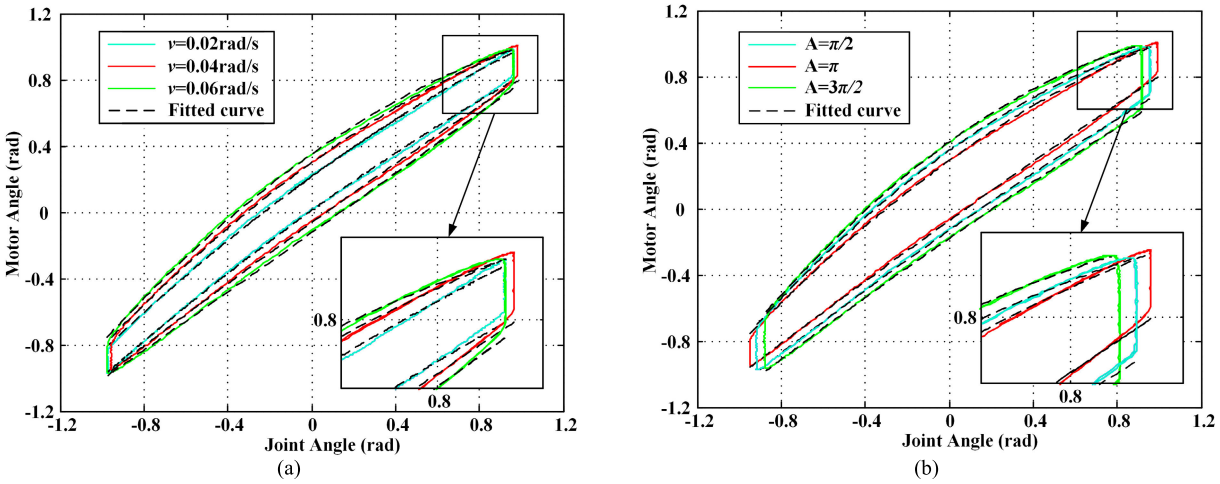

FIGURE 11. Parameter identification under different conditions. (a) Motion velocities. (b) Bending angles.

of elastic component, and the performance is sufficient for practical application.

V. COMPLIANT CONTROL

The vast majority of industrial robots work according to pre-programmed tasks and cannot respond to changes in external conditions. As an essential feature of next-generation robots, compliant control is widely applied for dynamic interactions between robots and their physical environments [32]. To test the performance of the proposed method, several experiments, including collision detection and hand guiding, were completed using the experimental setup illustrated in Fig. 4. The video of the experimental validations is available online.[2]

A. COLLISION DETECTION

The main function of collision detection is to reduce the impact of collision forces on the robot body. When the change of the external conditions is monitored, the robot will respond immediately. To ensure safety, the disturbance needs to be observed in real time. When the monitor value exceeds a certain threshold, it can be considered that a physical collision occurs in the joint. Thus, the motor will respond quickly to mitigate the damage.

Fig. 13 shows the scheme of collision detection; a closed-loop control of the drive motor is formed by the motor encoder, and θ_c is obtained and outputted to form a second closed-loop control. The drive motor is commanded to follow a sinusoid signal under a mode of position control. An overall collision detection procedure is shown in Algorithm 1. The relationship of position transmission is identified without disturbance and saved as the model to calculate the estimated motor angle first. Then, when the system runs, the minimal difference δ between the measured and ideal motor angle is monitored in real time. δ_a is the maximum allowable error; if $|\delta| \leq \delta_a$, the system will run normally, and if $|\delta| \leq \delta_a$, the motor will stop rotating. As shown in Fig. 12(a), a wooden

[2]. https://youtu.be/GYgpqAcITTg

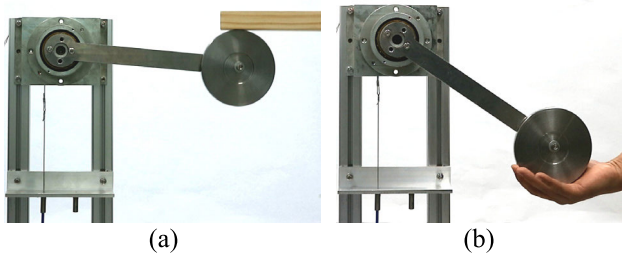

FIGURE 12. Experimental setup. (a) Collision detection. (b) Hand guiding.

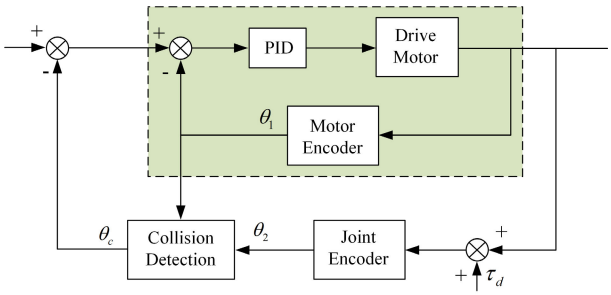

FIGURE 13. Controller diagram of collision detection.

stick is used to hit the load plate, producing a sudden torque τ_d. The collision results are demonstrated in Fig. 15, and as seen, the joint angle and transmission characteristics have conspicuous displacement transmission errors due to the elasticity of the tendon when a collision occurs.

Algorithm 1 Collision Detection

$\theta_{1r}(t) = P_r\hat{\theta}_2^2(t) + Q_r\hat{\theta}_2(t) + M_r$
$\theta_{1p}(t) = P_p\hat{\theta}_2^2(t) + Q_p\hat{\theta}_2(t) + M_p$
if $|\theta_{1p}(t) - \theta_1(t)| < |\theta_{1r}(t) - \theta_1(t)|$ **then**
$\delta = \theta_{1p}(t) - \theta_1(t)$;$\theta_1'(t) = \theta_{1p}(t_-)$
else $\delta = \theta_{1r}(t) - \theta_1(t)$;$\theta_1'(t) = \theta_{1r}(t_-)$
end if
If $|\delta| \le \delta_a$ **then**
$\theta_c(t) = \theta_1'(t)$
else $\theta_c(t) = \theta_1(t_-)$
end if

B. HAND GUIDING

The goal of hand guiding is to drag the robot directly and manually. When the external conditions change, the manipulator will move accordingly. At present, robot teaching mainly depends on workers operating the teaching device to complete the training. However, there are many defects in this approach, such as low teaching efficiency, complex teaching processes, and the need for operators to master certain knowledge of robotic use. Backdrivabilty means that the operator can directly drag each joint of the manipulator, move it to the ideal posture and record it. Using physical human-robot interaction, this kind of teaching method can avoid the

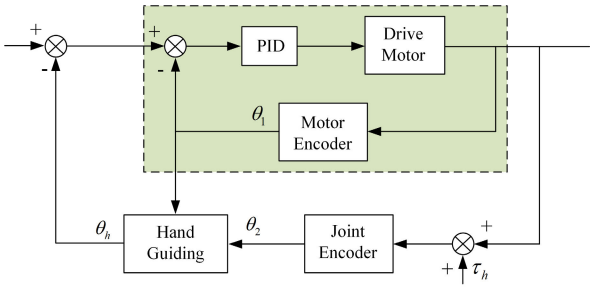

FIGURE 14. Controller diagram of hand guiding.

numerous shortcomings of traditional teaching, which is a promising technology in robotic design.

Algorithm 2 Hand Guiding

$\theta_{1r}(t) = P_r\hat{\theta}_2^2(t) + Q_r\hat{\theta}_2(t) + M_r$
$\theta_{1p}(t) = P_p\hat{\theta}_2^2(t) + Q_p\hat{\theta}_2(t) + M_p$
if $|\theta_{1p}(t) - \theta_1(t)| < |\theta_{1r}(t) - \theta_1(t)|$ **then**
$\theta_h(t) = \theta_{1p}(t)$
else $\theta_h(t) = \theta_{1r}(t)$
end if

The scheme of hand guiding is illustrated in Fig. 14; dual closed-loop control of the drive motor is also formed by the motor encoder and the joint encoder. An overall procedure of hand guiding is shown in Algorithm 2. The relationship of position transmission is also identified and saved without a disturbing force. The system remains in a stationary state without external force. When there is external torque τ_h, the joint angle will change due to the elasticity, and the estimated value of the motor angle also varies according to (19). Finally, the motor will rotate to the nearest value θ_h. As shown in Fig. 12(b), the joint can be moved by hand. The results are displayed in Fig. 16, and as seen, the joint is dragged for three cycles. Every cycle includes both upward and downward actions. The motor can move following the change of the joint angle. Due to the existence of backlash, the error is greatest when the direction changes.

C. FREQUENCY CHARACTERISTICS OF COMPLIANT CONTROL

The nonlinear characteristic of single tendon-sheath transmission can negatively influence the control bandwidth of the system. To evaluate the control performance of the proposed method, tracking experiments with various sinusoidal frequencies were carried out using the experimental setup shown in Fig. 4. The total sheath bending angle was set to $\pi/2$, π, and $3\pi/2$ to determine the control performance in different tendon-sheath configurations. The Bode diagrams of frequency characteristics for compliant control are shown in Fig. 17; it is obvious that the bandwidth of the control system is approximately 6Hz, and the system bandwidth

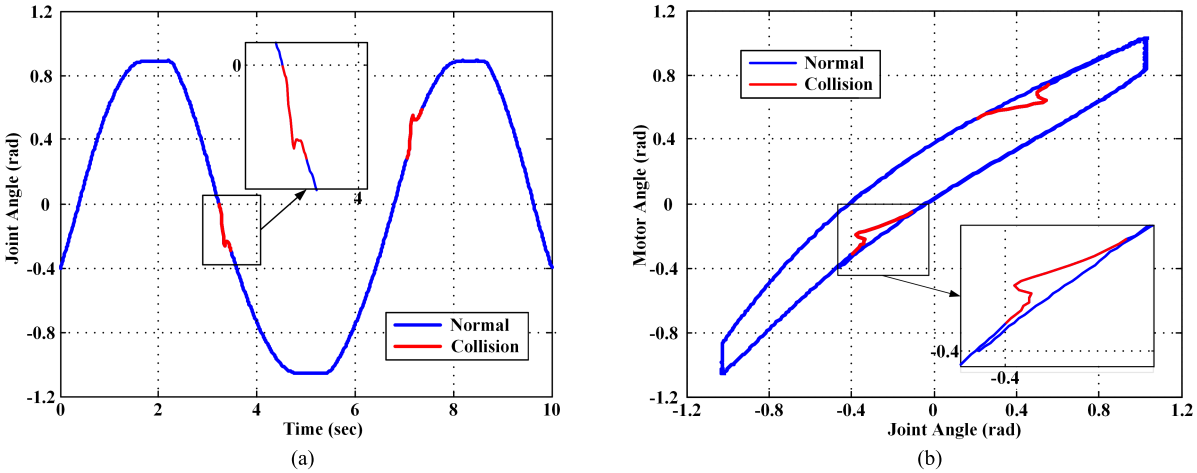

FIGURE 15. The results of the collision detection experiment. (a) Joint angle. (b) Transmission characteristics.

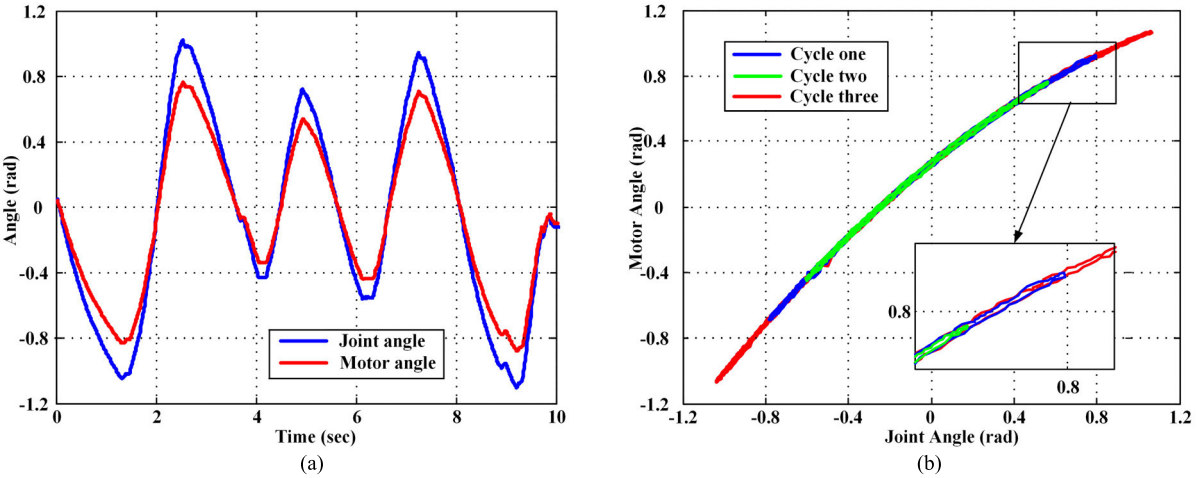

FIGURE 16. The results of the hand guiding experiment. (a) Joint angle. (b) Transmission characteristics.

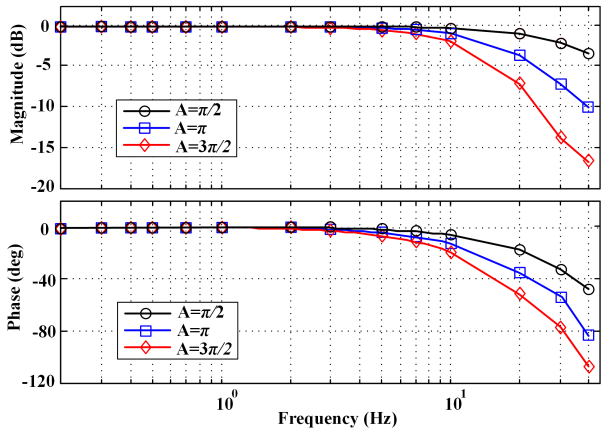

FIGURE 17. Compliant frequency responses with different total sheath bending angle.

will decrease with the increase of the total sheath bending angle.

VI. CONCLUSION

This paper has put forward a systematic new approach for compliant controls in single TSAs. The displacement transmission model was established on the basis of the force transmission model, which can be applied for the control of a tendon-sheath system under an arbitrary fixed shape. An experimental setup was designed to test the proposed method, and the transmission processes were further assessed during the sinusoidal wave input signal. Comparisons between experimental results and fitted curves are presented. The parameters of the position transmission model were identified based on offline measurements using dual encoders installed at the drive motor and the actuated joint. Based on the model, the compliant controllers were designed to control the contact performance between the actuated joint and the environment, using only two position sensors on the motor side and the joint side. The effectiveness of the presented method was validated by compliant control experiments, including collision detection and hand guiding. The results show that the transmission model and the parameter identification are available, and the function of compliant control can be realized. The change in the torque will affect the transmission characteristics. In the absence of force sensors, torque can be detected by the characteristics of position transmission. This approach is particularly suitable for robots

actuated by TSAs, such as rehabilitation robots, exoskeletons and manipulators.

Compliance control experiments were performed under the assumption of a fixed sheath shape. When TSAs are applied to a serial multiple-joint robot, the sheath will frequently vary during the task. Consequently, more complex algorithms, such as a fuzzy logic control strategy or neural network control strategy, will be applied considering the variation of curvature in future work. Furthermore, torque estimation and compliant control of double TSAs will be studied.

REFERENCES

[1] G. A. Pratt and M. W. Williamson, "Series elastic actuators," in *Proc. IEEE/RSJ Int. Conf. Intell. Robots Syst. (IROS)*, Pittsburgh, PA, USA, pp. 399–406, Aug. 1995.

[2] M. Kaneko, M. Wada, H. Maekawa, and K. Tanie, "A new consideration on tendon-tension control system of robot hands," in *Proc. IEEE Int. Conf. Robot. Autom.*, Dec. 2002, pp. 1028–1033.

[3] M. Kaneko, W. Paetsch, and H. Tolle, "Input-dependent stability of joint torque control of tendon-driven robot hands," *IEEE Trans. Ind. Electron.*, vol. 39, no. 2, pp. 96–104, Apr. 1992.

[4] S. J. Phee, S. C. Low, Z. L. Sun, K. Y. Ho, W. M. Huang, and Z. M. Thant, "Robotic system for no-scar gastrointestinal surgery," *Int. J. Med. Robot. Comput. Assist. Surg.*, vol. 4, no. 1, pp. 15–22, Mar. 2008.

[5] S. J. Phee, S. C. Low, P. Dario, and A. Menciassi, "Tendon sheath analysis for estimation of distal end force and elongation for sensorless distal end," *Robotica*, vol. 28, no. 7, pp. 1073–1082, Dec. 2010.

[6] S. Grosu, L. De Rijcke, V. Grosu, J. Geeroms, B. Vanderboght, D. Lefeber, and C. Rodriguez-Guerrero, "Driving robotic exoskeletons using cable-based transmissions: A qualitative analysis and overview," *Appl. Mech. Rev.*, vol. 70, no. 6, 2019, Art. no. 060801.

[7] K. Kong and D. Jeon, "Design and control of an exoskeleton for the elderly and patients," *IEEE/ASME Trans. Mechatronics*, vol. 11, no. 4, pp. 428–432, Aug. 2006.

[8] K. Kong, J. Bae, and M. Tomizuka, "Torque mode control of a cable driven actuating system by sensor fusion," *J. Dyn. Syst. Meas. Control*, vol. 135, no. 3, 2013, Art. no. 031003.

[9] P. Agarwal and A. D. Deshpande, "Series elastic actuators for small-scale robotic applications," *J. Mech. Robot.*, vol. 9, no. 3, 2017, Art. no. 031016.

[10] P. Agarwal, J. Fox, Y. Yun, M. K. O'Malley, and A. D. Deshpande, "An index finger exoskeleton with series elastic actuation for rehabilitation: Design, control and performance characterization," *Int. J. Robot. Res.*, vol. 34, no. 14, pp. 1747–1772, Dec. 2015.

[11] Q. Wu, X. Wang, B. Chen, and H. Wu, "Design and fuzzy sliding mode admittance control of a soft wearable exoskeleton for elbow rehabilitation," *IEEE Access*, vol. 6, pp. 60249–60263, 2018.

[12] Q. Wu, B. Chen, and H. Wu, "Adaptive admittance control of an upper extremity rehabilitation robot with neural-network-based disturbance observer," *IEEE Access*, vol. 7, pp. 123807–123819, 2019.

[13] H. Vallery, J. Veneman, E. Van Asseldonk, R. Ekkelenkamp, M. Buss, and H. Van Der Kooij, "Compliant actuation of rehabilitation robots," *IEEE Robot. Automat. Mag.*, vol. 15, no. 3, pp. 60–69, Sep. 2008.

[14] J. F. Veneman, R. Ekkelenkamp, R. Kruidhof, F. C. T. Van Der Helm, and H. Van Der Kooij, "A series elastic- and Bowden-cable-based actuation system for use as torque actuator in exoskeleton-type robots," *Int. J. Robot. Res.*, vol. 25, no. 3, pp. 261–281, Mar. 2006.

[15] Y. Sakagami, R. Watanabe, C. Aoyama, S. Matsunaga, N. Higaki, and K. Fujimura, "The intelligent ASIMO: System overview and integration," in *Proc. IEEE/RSJ Int. Conf. Intell. Robots Syst.* Lausanne, Switzerland, Jun. 2003, pp. 2478–2483.

[16] S. Park, H. Lee, D. Hanson, and P. Y. Oh, "Sophia-Hubo's arm motion generation for a handshake and gestures," in *Proc. 15th Int. Conf. Ubiquitous Robots (UR)*, Honolulu, HI, USA, Jun. 2018, pp. 511–515.

[17] Anonymous, "ABB introduces YuMi a dual-arm co-robot," *Manuf. Eng.*, vol. 154, no. 6, p. 22, 2015.

[18] T. Wimbock, D. Nenchev, A. Albu-Schaffer, and G. Hirzinger, "Experimental study on dynamic reactionless motions with DLR's humanoid robot Justin," in *Proc. IEEE/RSJ Int. Conf. Intell. Robots Syst.*, St. Louis, MO, USA, Oct. 2009, pp. 5481–5486.

[19] E. Guizzo and E. Ackerman. *How Rethink Robotics Built Its New Baxter Robot Worker*. [Online]. Available: http://spectrum.ieee.org/robotics/industrial-robots/rethink-robotics baxter-robot-factory-worker

[20] V. Maheu, J. Frappier, P. S. Archambault, and F. Routhier, "Evaluation of the JACO robotic arm: Clinico-economic study for powered wheelchair users with upper-extremity disabilities," in *Proc. IEEE Int. Conf. Rehabil. Robot.*, Piscataway, NJ, USA, Jun. 2011, pp. 1–5.

[21] K. Salisbury, W. Townsend, B. Ebrman, and D. Dipietro, "Preliminary design of a whole-arm manipulation system (WAMS)," in *Proc. IEEE Int. Conf. Robot. Autom.*, Philadelphia, PA, USA, Jan. 2003, pp. 254–260.

[22] Y.-J. Kim, "Anthropomorphic low-inertia high-stiffness manipulator for high-speed safe interaction," *IEEE Trans. Robot.*, vol. 33, no. 6, pp. 1358–1374, Dec. 2017.

[23] V. Villani, F. Pini, F. Leali, and C. Secchi, "Survey on human–robot collaboration in industrial settings: Safety, intuitive interfaces and applications," *Mechatronics*, vol. 55, pp. 248–266, Nov. 2018.

[24] A. Hentout, M. Aouache, A. Maoudj, and I. Akli, "Human–robot interaction in industrial collaborative robotics: A literature review of the decade 2008–2017," *Adv. Robot.*, vol. 33, nos. 15–16, pp. 764–799, Aug. 2019.

[25] N. Hogan, "Impedance control: An approach to manipulation," in *Proc. Amer. Control Conf.*, Jul. 1984, pp. 304–313.

[26] A. Q. L. Keemink, H. Van Der Kooij, and A. H. A. Stienen, "Admittance control for physical human-robot interaction," *Int. J. Robot. Res.*, vol. 37, no. 11, pp. 1421–1444, 2018.

[27] L. Roveda, "Adaptive interaction controller for compliant robot base applications," *IEEE Access*, vol. 7, pp. 6553–6561, 2019.

[28] F. Zeng, J. Xiao, and H. Liu, "Force/torque sensorless compliant control strategy for assembly tasks using a 6-DOF collaborative robot," *IEEE Access*, vol. 7, pp. 108795–108805, 2019.

[29] A. Calanca, R. Muradore, and P. Fiorini, "A review of algorithms for compliant control of stiff and fixed-compliance robots," *IEEE/ASME Trans. Mechatronics*, vol. 21, no. 2, pp. 613–624, Apr. 2016.

[30] *Robots and Robotic Devices—Safety Requirements for Industrial Robots—Part 1: Robots*, Standard ISO 10218-1:2011, 2011.

[31] *Robots and Robotic Devices—Safety Requirements for Industrial Robots—Part 2: Robot Systems and Integration*, 2011.

[32] A. Albu-Schäeffer, S. Haddadin, C. Ott, A. Stemmer, T. Wimböck, and G. Hirzinger, "The DLR lightweight robot: Design and control concepts for robots in human environments," *Ind. Robot*, vol. 34, no. 5, pp. 376–385, Aug. 2007.

[33] S. Haddadin, A. De Luca, and A. Albu-Schaffer, "Robot collisions: A survey on detection, isolation, and identification," *IEEE Trans. Robot.*, vol. 33, no. 6, pp. 1292–1312, Dec. 2017.

[34] F. Min, G. Wang, and N. Liu, "Collision detection and identification on robot manipulators based on vibration analysis," *Sensors*, vol. 19, no. 5, p. 1080, Mar. 2019.

[35] Y. Ogura, M. Fujii, K. Nishijima, H. Murakami, and M. Sonehara, "Applicability of hand-guided robot for assembly-line work," *J. Robot. Mechatron.* , vol. 24, no. 3, pp. 547–552, Jun. 2012.

[36] M. Fujii, H. Murakami, and M. Sonehara, "Study on application of a human-robot collaborative system using hand-guiding in a production line," *IHI Eng. Rev.*, vol. 49, no. 1, pp. 24–29, 2016.

[37] S. Zhang, S. Wang, F. Jing, and M. Tan, "A sensorless hand guiding scheme based on model identification and control for industrial robot," *IEEE Trans. Ind. Informat.*, vol. 15, no. 9, pp. 5204–5213, Sep. 2019.

[38] Q. Wu, X. Wang, L. Chen, and F. Du, "Transmission model and compensation control of double-tendon-sheath actuation system," *IEEE Trans. Ind. Electron.*, vol. 62, no. 3, pp. 1599–1609, Mar. 2015.

[39] L. Chen, X. Wang, and W. L. Xu, "Inverse transmission model and compensation control of a single-tendon–sheath actuator," *IEEE Trans. Ind. Electron.*, vol. 61, no. 3, pp. 1424–1433, Mar. 2014.

[40] H. X. Nguyen, T. N.-C. Tran, J. W. Park, and J. W. Jeon, "Auto-calibration and noise reduction for the sinusoidal signals of magnetic encoders," in *Proc. 43rd Annu. Conf. IEEE Ind. Electron. Soc. (IECON)*, Beijing, China, Oct. 2017, pp. 3286–3291.

[41] H. X. Nguyen, T. N.-C. Tran, J. W. Park, and J. W. Jeon, "An adaptive linear-neuron-based third-order PLL to improve the accuracy of absolute magnetic encoders," *IEEE Trans. Ind. Electron.*, vol. 66, no. 6, pp. 4639–4649, Jun. 2019.

MENG YIN was born in Taian, Shangdong, China, in 1992. He is currently pursuing the Ph.D. degree with the University of Chinese Academy of Sciences, China. He is a member of the Intelligent Equipment and Production Line Laboratory, Shenyang Institute of Automation, Chinese Academy of Sciences. The team's research activities include aerospace simulators, intelligent manufacturing, and intelligent robots. His research interests include tendon-sheath driven humanoid robots, mechanical design and optimization, and compliant control.

HAOTING WU was born in Qingdao, Shangdong, China, in 1993. He received the bachelor's degree from the China University of Mining and Technology, in 2016. He is currently pursuing the master's degree in mechanical engineering with Northeastern University, China. He is a member of the Intelligent Equipment and Production Line Laboratory, Shenyang Institute of Automation, Chinese Academy of Sciences. The team's research activities include aerospace simulators and intelligent robots. His research interests include tendon-sheath driven humanoid robots, friction compensation control, and compliance control.

ZHIGANG XU received the Ph.D. degree from the University of Chinese Academy of Sciences, in 2008. He is currently a member of State Key Laboratory of Robotics, Chinese Academy of Sciences, where he is also the Head of the Intelligent Equipment and Production Line Laboratory, Shenyang Institute of Automation. He has published over 80 technique papers and is the holder of 130 Chinese patents in these areas. He presided over and completed many major aerospace test system research and application projects, such as the National 863 program, national major science and technology projects, space station projects, lunar exploration projects, and deep space exploration. His current research interests include robotic mechanism, high precision measurement and control of force/position, spacecraft ground simulation test technology and equipment, intelligent manufacturing, and intelligent factory planning and construction.

WEI HAN was born in Tangshan, Hebei, China, in 1993. He received the bachelor's degree from the China University of Geosciences, Wuhan, in 2016. He is currently pursuing the master's degree in mechanical design and manufacturing with Northeastern University. He is a member of the Intelligent Equipment and Production Line Laboratory, Shenyang Institute of Automation, Chinese Academy of Sciences. The team's research activities include aerospace simulators, intelligent manufacturing, and intelligent robots. His research interests include dexterous hand base on tendon-sheath actuators, structural optimization, transmission characteristics of tendon-sheath, dynamics simulation, and grab algorithm.

ZHILIANG ZHAO was born in Huaian, Jiangsu, China, in 1995. He received the bachelor's degree from Hohai University, in 2018. He is currently pursuing the master's degree in mechanical engineering with Northeastern University, China. He is a member of the Intelligent Equipment and Production Line Laboratory, Shenyang Institute of Automation, Chinese Academy of Sciences. The team's research activities include aerospace simulators, intelligent manufacturing, and intelligent robots. His research interests include tendon-sheath driven humanoid robots, computer virtual simulation, and compliant control.